Supporting Information

Vibrations of Dimers of Mechanically Coupled Nanostructures: Analytical and Numerical Modeling

Jean Lermé, Jérémie Margueritat, and Aurélien Crut*

Université de Lyon, CNRS, Université Claude Bernard Lyon 1, Institut Lumière Matière, F-69622 Villeurbanne, France

Corresponding author

***E-mail: aurelien.crut@univ-lyon1.fr**

Contents

The slab model

Preliminaries

In this Section we describe the analytical one-dimensional "slab model" (SM) which, despite its simplicity, allows analysing thoroughly the numerical FEM results reported in the main text on several homogeneous or composite mechanical nanostructures. In the SM the systems consist of, either a single homogeneous slab, or a stacking of mechanically-coupled parallel planar homogeneous slabs, each having an infinite extent in both transverse *x* and *y* directions (namely, those defining the planar surfaces of the slabs). The translation invariance of the "nanostructure" geometries along the *x* and *y* directions allows a very simple analytical model to be built. The two system geometries involved in the present work are depicted in Figure S1.

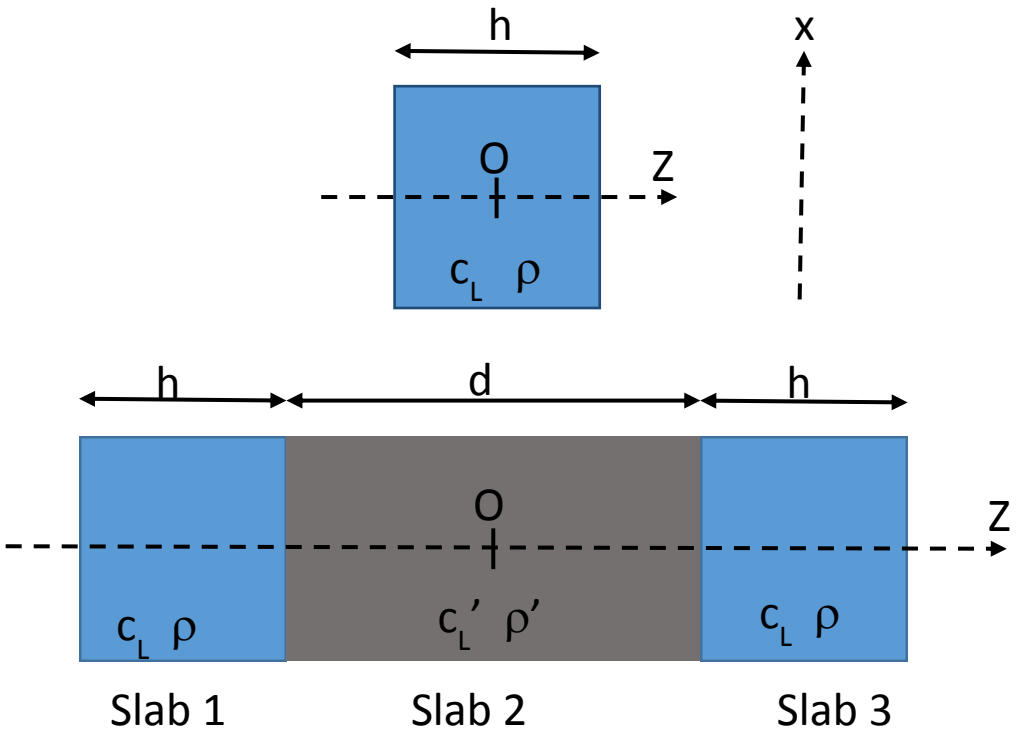

Figure S1: System geometries involved in this work: (1) a single slab of thickness *h* (upper figure); (2) a "homodimer" of slabs (lower figure), consisting of two identical slabs (slabs 1 and 3) of thickness *h*, mechanically coupled by a third slab (slab 2) made of a different material, of thickness *d*. Translation invariance in the transverse *x*-*y* plane is assumed. c_L and ρ (c_L' and ρ') are the longitudinal sound velocity and mass density characterizing the materials.

Even though the systems are far from representing realistic finite three-dimensional nanostructures, as nano-cylinders for instance (see Figures in the main text), we will see that the physics of the SM underlies most general features of the numerical FEM results in the regime where shear and axial motions are uncoupled.

Each slab is made of a homogeneous linear isotropic purely elastic medium characterized by its mass density ρ and a pair of independent elastic parameters which can be either λ and μ [first and second (shear) Lamé coefficients], $c_{L,T}$ (longitudinal and transverse sound velocities), or ν (Poisson coefficient) and E (Young modulus). Because the lateral extents of the slabs, along the x and y directions, are assumed infinite, the transverse (shear) and longitudinal (dilatation/compressional) motions and their corresponding vibrational eigenmodes can be analysed separately. Here, only the longitudinal motion along the z direction, and associated vibrational eigenmodes, are addressed. Thus only the parameters ρ and $c_L = ((\lambda + 2\mu)/\rho)^{1/2}$ will be involved.

In the case of one-dimensional motion along the z-direction, and in the absence of body force density, the displacement field $u(z,t)$ is governed by the Navier's equation [1]

$$\frac{\partial^2 u(z,t)}{\partial t^2} = c_L^2 \frac{\partial^2 u(z,t)}{\partial z^2} \tag{1}$$

Actually, in this simple specific case, the Navier's equation is nothing but a mere one-dimensional wave equation. Searching for harmonic solutions of the form $u(z,t) = u(z)e^{-i\omega t}$, the Navier's equation expresses as

$$\frac{\partial^2 u(z)}{\partial z^2} + \frac{\omega^2}{c_L^2} u(z) = 0 \tag{2}$$

The stress component for longitudinal motion, $t(x)$, is given by [1]

$$t(z) = \rho c_L^2 \frac{\partial u(z)}{\partial z} \tag{3}$$

A) Single slab (see Figure S1; upper panel)

The solutions of eqs. (2) and (3) are

$$u(z) = A\cos(\frac{\omega z}{c_L}) + B\sin(\frac{\omega z}{c_L}) \tag{4}$$

$$t(z) = \rho c_L \omega[-A\sin(\frac{\omega z}{c_L}) + B\cos(\frac{\omega z}{c_L})] \tag{5}$$

Various sets of eigenmodes can be defined, depending of the boundary conditions imposed at both interfaces $z = \pm h/2$, where h is the slab thickness along the z direction. Three sets of boundary conditions will be considered here:

Case 1) Stress-free conditions: $t(\pm h/2) = 0$
Case 2) Displacement-free conditions: $u(\pm h/2) = 0$
Case 3) Hybrid boundary conditions: [$t(-h/2) = 0$; $u(h/2) = 0$] or [$u(-h/2) = 0$; $t(h/2) = 0$]

Stress-free boundary conditions are relevant when dealing with objects in vacuum or, approximately, for describing interfaces separating the object from a medium with a much smaller acoustic impedance. Conversely, displacement-free boundary conditions correspond to the limit case of an interface with a medium of much larger acoustic impedance [2]. All the three considered cases are relevant for analysing vibrational eigenmodes of composite systems involving several mechanically-coupled subunits, or stacked slabs, in vacuum.

In each case, the two boundary conditions [obtained by using eqs. (4) and/or (5)] lead to a homogeneous linear system of two equations relating the unknown coefficients *A* and *B*. The eigen-frequencies are the (real) ω-values ensuring a non-zero solution. They are thus determined in searching the zeros of the 2×2 determinant (denoted Δ below) of the homogeneous linear system. For a single slab the computations are quite straightforward, and we provide only the final results. One obtains

Case 1)

$$\Delta = \sin(\frac{\omega h}{c_L}) \qquad \omega_n = n\frac{\pi\, c_L}{h} \qquad \text{where } n \text{ is an integer } (n \geq 0) \qquad (6)$$

The $n = 0$ mode corresponds to a mere rigid translation of the slab as a whole, and can be paralleled with the fundamental $l = 1$ mode (referred to as the translational mode) for a sphere [1].

■ n odd ($n = 2n' + 1$; $n' = 0, 1, 2, 3, \ldots$)

Normalized displacement field $\quad \bar{u}_n(z) = \sqrt{\frac{2}{h}}\sin(\frac{n\pi}{h}z) \qquad (7)$

These modes will be referred to as the "symmetric modes" [$\bar{u}_n(-z) = -\bar{u}_n(z)$]. For such modes the arrows picturing the displacement fields $\bar{u}_n(z<0)$ and $\bar{u}_n(z>0)$ are mirror images from each other relative to the *x-y* median plane at $z = 0$.

■ n even ($n = 2n'$; $n' = 1, 2, 3, \ldots$)

Normalized displacement field $\quad \bar{u}_n(z) = \sqrt{\frac{2}{h}}\cos(\frac{n\pi}{h}z) \qquad (8)$

These modes will be referred to as the "antisymmetric modes" [$\bar{u}_n(-z) = \bar{u}_n(z)$].

The normalization of the displacement field is conventionally defined here by the condition

$$\int_{-h/2}^{h/2} \bar{u}_n^2(z)dz = 1 \qquad (9)$$

Case 2)

$$\Delta = \sin(\frac{\omega h}{c_L}) \qquad \omega_n = n\frac{\pi\, c_L}{h} \qquad \text{where } n \text{ is an integer } (n > 0) \text{ [same eigenfrequencies as in Case 1)]} \qquad (10)$$

■ n odd ($n = 2n' + 1$; $n' = 0, 1, 2, 3, \ldots$)

Normalized displacement field $\bar{u}_n(z) = \sqrt{\frac{2}{h}} \cos(\frac{n\pi}{h} z)$ (11)

These modes are antisymmetric (see the definition above)

■ n even ($n = 2n'$; $n' = 1, 2, 3, \ldots$)

Normalized displacement field $\bar{u}_n(z) = \sqrt{\frac{2}{h}} \sin(\frac{n\pi}{h} z)$ (12)

These modes are symmetric (see the definition above).

Case 3)

■ $t(-h/2) = 0$; $u(h/2) = 0$

$\Delta = \cos(\frac{\omega h}{c_L})$ $\omega_n = (n + \frac{1}{2}) \frac{\pi c_L}{h}$ ($n = 0, 1, 2, 3, \ldots$) (13)

Normalized displacement field $\bar{u}_n(z) = \frac{1}{\sqrt{h}} [\cos((n + \frac{1}{2}) \frac{\pi z}{h}) - (-1)^n \sin((n + \frac{1}{2}) \frac{\pi z}{h})]$ (14)

■ $u(-h/2) = 0$; $t(h/2) = 0$

$\Delta = \cos(\frac{\omega h}{c_L})$ $\omega_n = (n + \frac{1}{2}) \frac{\pi c_L}{h}$ ($n = 0, 1, 2, 3, \ldots$) (15)

Normalized displacement field $\bar{u}_n(z) = \frac{1}{\sqrt{h}} [\cos((n + \frac{1}{2}) \frac{\pi z}{h}) + (-1)^n \sin((n + \frac{1}{2}) \frac{\pi z}{h})]$ (16)

B) Homodimer (see Figure S1; lower panel)

The composite system consists of two identical slabs, of thickness h, separated by a slab of thickness d [the parameters associated with this second material are labelled with a *prime* symbol, i.e. ρ', c_L']. The x-y plane at $z = 0$ is the median plane of the overall homodimer. The displacement fields and corresponding stress components in each slab are written as

Slab 1: $-(h + d/2) < z < -d/2$

$u_1(z) = A_1 \cos(\frac{\omega}{c_L} z) + B_1 \sin(\frac{\omega}{c_L} z)$ (17)

$t_1(z) = \rho c_L \omega [-A_1 \sin(\frac{\omega}{c_L} z) + B_1 \cos(\frac{\omega}{c_L} z)]$ (18)

Slab 2 (second material): $-d/2 < z < d/2$

$$u_2(z) = A_2 \cos(\frac{\omega}{c_L'} z) + B_2 \sin(\frac{\omega}{c_L'} z) \quad (19)$$

$$t_2(z) = \rho' c_L' \omega[-A_2 \sin(\frac{\omega}{c_L'} z) + B_2 \cos(\frac{\omega}{c_L'} z)] \quad (20)$$

Slab 3: $d/2 < z < h + d/2$

$$u_3(z) = A_3 \cos(\frac{\omega}{c_L} z) + B_3 \sin(\frac{\omega}{c_L} z) \quad (21)$$

$$t_3(z) = \rho c_L \omega[-A_3 \sin(\frac{\omega}{c_L} z) + B_3 \cos(\frac{\omega}{c_L} z)] \quad (22)$$

The boundary conditions at the four interfaces (two external and two internal) are

External Interface (n° 1): $z_1 = -h - d/2$

stress-free condition: $t_1(z_1) = 0$

Internal Interface (n° 2): $z_2 = -d/2$

continuity of the displacement field and stress: $u_1(z_2) = u_2(z_2)$ and $t_1(z_2) = t_2(z_2)$

Internal Interface (n° 3): $z_3 = d/2$

continuity of the displacement field and stress: $u_2(z_3) = u_3(z_3)$ and $t_2(z_3) = t_3(z_3)$

External Interface (n° 4): $z_4 = h + d/2$

stress-free condition: $t_3(z_4) = 0$

From these six boundary conditions one obtains the following homogeneous linear system of equations relating the six unknown coefficients A_i and B_i

$$A_1 \sin(\frac{\omega}{c_L} \frac{a}{2}) + B_1 \cos(\frac{\omega}{c_L} \frac{a}{2}) = 0 \quad (23)$$

$$A_1 \cos(\frac{\omega}{c_L} \frac{d}{2}) - B_1 \sin(\frac{\omega}{c_L} \frac{d}{2}) - A_2 \cos(\frac{\omega}{c_L'} \frac{d}{2}) + B_2 \sin(\frac{\omega}{c_L'} \frac{d}{2}) = 0 \quad (24)$$

$$A_1 \sin(\frac{\omega}{c_L}\frac{d}{2}) + B_1 \cos(\frac{\omega}{c_L}\frac{d}{2}) - p\,[A_2 \sin(\frac{\omega}{c_L'}\frac{d}{2}) + B_2 \cos(\frac{\omega}{c_L'}\frac{d}{2})] = 0 \quad (25)$$

$$A_3 \cos(\frac{\omega}{c_L}\frac{d}{2}) + B_3 \sin(\frac{\omega}{c_L}\frac{d}{2}) - A_2 \cos(\frac{\omega}{c_L'}\frac{d}{2}) - B_2 \sin(\frac{\omega}{c_L'}\frac{d}{2}) = 0 \quad (26)$$

$$-A_3 \sin(\frac{\omega}{c_L}\frac{d}{2}) + B_3 \cos(\frac{\omega}{c_L}\frac{d}{2}) - p\,[-A_2 \sin(\frac{\omega}{c_L'}\frac{d}{2}) + B_2 \cos(\frac{\omega}{c_L'}\frac{d}{2})] = 0 \quad (27)$$

$$-A_3 \sin(\frac{\omega}{c_L}\frac{a}{2}) + B_3 \cos(\frac{\omega}{c_L}\frac{a}{2}) = 0 \quad (28)$$

where $a = d + 2h$ is the overall length of the homodimer and $p = \frac{c_L'}{c_L}\frac{\rho'}{\rho} = \frac{Z'}{Z}$ is the acoustic impedance ratio.

The problem in hand can be drastically simplified in taking into account the symmetry property of the homodimer geometry (the system is symmetric with respect to the median transverse plane located at $z = 0$). Symmetric modes $[u(-z) = -u(z)]$ are determined by imposing the constraints $A_3 = -A_1$, $B_3 = B_1$ and $A_2 = 0$, whereas antisymmetric modes $[(u(-z) = u(z)]$ are determined by imposing the constraints $B_3 = -B_1$, $A_3 = A_1$ and $B_2 = 0$. For both cases (symmetric or antisymmetric character) the first three equations (23-25) are independent, the last three others (26-28) being equal to the previous ones. In both cases the eigenfrequencies are thus the zeros of a 3×3 determinant.

Symmetric modes:

$$\begin{vmatrix} \sin(\frac{\omega}{c_L}\frac{a}{2}) & \cos(\frac{\omega}{c_L}\frac{a}{2}) & 0 \\ \cos(\frac{\omega}{c_L}\frac{d}{2}) & -\sin(\frac{\omega}{c_L}\frac{d}{2}) & \sin(\frac{\omega}{c_L'}\frac{d}{2}) \\ \sin(\frac{\omega}{c_L}\frac{d}{2}) & \cos(\frac{\omega}{c_L}\frac{d}{2}) & -p\cos(\frac{\omega}{c_L'}\frac{d}{2}) \end{vmatrix} = 0$$

Introducing the convenient dimensionless quantity

$$\xi = \frac{\omega h}{c_L} \quad (29)$$

one obtains straightforwardly

$$p\cos(\frac{c_L}{c_L'}\frac{d}{2h}\xi)\cos(\xi) - \sin(\frac{c_L}{c_L'}\frac{d}{2h}\xi)\sin(\xi) = 0 \quad (30)$$

The consistency of this equation can be checked in analysing two limiting cases

● When $d = 0$ (the slabs 1 and 3 are in mechanical contact) eq. (30) reduces to

$$\cos(\xi) = \cos(\omega h / c_L) = 0 \;\rightarrow\; \xi = \frac{\omega h}{c_L} = (2n+1)\frac{\pi}{2} \quad (n = 0, 1, 2, 3\ ..) \;\rightarrow\; \omega = (2n+1)\frac{\pi\, c_L}{(2h)}$$

As expected one obtains the eigenfrequencies of the symmetric modes of a single slab of thickness $2h$ in vacuum (stress-free conditions at both ends).

● When the three slabs are made of the same material ($p = 1$, $\frac{c_L}{c_L'} = 1$), eq. (30) reduces to

$$\cos(\frac{d}{2h}\xi)\cos(\xi) - \sin(\frac{d}{2h}\xi)\sin(\xi) = \cos((\frac{d}{2h}+1)\xi) = \cos(\frac{a}{2h}\xi) = 0$$

$$\rightarrow \frac{a}{2h}\xi = \frac{a}{2h}\frac{\omega h}{c_L} = (2n+1)\frac{\pi}{2} \quad (n = 0, 1, 2, 3\ \ldots.) \;\rightarrow\; \omega = (2n+1)\frac{\pi\, c_L}{a}$$

As expected one obtains the eigenfrequencies of the symmetric modes of a single slab of thickness $a = d + 2h$ in vacuum (stress-free conditions at both interfaces).

For each eigenfrequency $\omega_i = c_L \xi_i / h$ the relative values of the three independent coefficients characterizing the displacement fields in the homodimer are

$$A_1 = -\frac{1}{\cos(\xi_i)}\cos(\xi_i \frac{a}{2h})\sin(\xi_i \frac{c_L}{c_L'}\frac{d}{2h})B_2 \quad ; \quad B_1 = \frac{1}{\cos(\xi_i)}\sin(\xi_i \frac{a}{2h})\sin(\xi_i \frac{c_L}{c_L'}\frac{d}{2h})B_2 \quad ; \quad B_2$$

$$\frac{B_1}{A_1} = -tg(\xi_i \frac{a}{2h})$$

Antisymmetric modes:

$$\begin{vmatrix} \sin(\frac{\omega}{c_L}\frac{a}{2}) & \cos(\frac{\omega}{c_L}\frac{a}{2}) & 0 \\ \cos(\frac{\omega}{c_L}\frac{d}{2}) & -\sin(\frac{\omega}{c_L}\frac{d}{2}) & -\cos(\frac{\omega}{c_L'}\frac{d}{2}) \\ \sin(\frac{\omega}{c_L}\frac{d}{2}) & \cos(\frac{\omega}{c_L}\frac{d}{2}) & -p\sin(\frac{\omega}{c_L'}\frac{d}{2}) \end{vmatrix} = 0$$

One obtains straightforwardly

$$p\sin(\frac{c_L}{c_L'}\frac{d}{2h}\xi)\cos(\xi)+\cos(\frac{c_L}{c_L'}\frac{d}{2h}\xi)\sin(\xi)=0 \qquad (31)$$

The consistency of this equation can be checked in analysing two limiting cases

● When d = 0 (no matrix; the slabs 1 and 3 are in mechanical contact) eq. (31) reduces to

$$\sin(\xi)=\sin(\omega h/c_L)=0 \;\rightarrow\; \xi=\frac{\omega h}{c_L}=n\pi \quad (n = 1, 2, 3 ..) \;\rightarrow\; \omega=(2n)\frac{\pi c_L}{(2h)}$$

As expected one obtains the eigenfrequencies of the antisymmetric modes of a single slab of thickness 2h in vacuum (stress-free conditions at both interfaces).

● When the three slabs are made of the same material (p = 1, $\frac{c_L}{c_L'}=1$), eq. (31) reduces to

$$\sin(\frac{d}{2h}\xi)\cos(\xi)+\cos(\frac{d}{2h}\xi)\sin(\xi)=\sin((\frac{d}{2h}+1)\xi)=\sin(\frac{a}{2h}\xi)=0$$

$$\rightarrow \frac{a}{2h}\xi=\frac{a}{2h}\frac{\omega h}{c_L}=n\pi \quad (n = 1, 2, 3 \ldots.) \;\rightarrow\; \omega=(2n)\frac{\pi c_L}{a}$$

As expected one obtains the eigenfrequencies of the antisymmetric modes of a single slab of thickness $a = d + 2h$ in vacuum (stress-free conditions at both interfaces).

For each eigenfrequency $\omega_i=c_L\xi_i/h$ the relative values of the three independent coefficients characterizing the displacement fields in the homodimer are

$$A_1=\frac{1}{\cos(\xi_i)}\cos(\xi_i\frac{a}{2h})\cos(\xi_i\frac{c_L}{c_L'}\frac{d}{2h})A_2 \quad ; \quad B_1=-\frac{1}{\cos(\xi_i)}\sin(\xi_i\frac{a}{2h})\cos(\xi_i\frac{c_L}{c_L'}\frac{d}{2h})A_2 \quad ; \quad A_2$$

$$\frac{B_1}{A_1}=-tg(\xi_i\frac{a}{2h})$$

<u>Additional remarks:</u>

<u>Remark 1</u>: As in the Lamb theory for an elastic sphere [1], where the eigenfrequencies of the (l,n,m) low-frequency vibrational modes scale as 1/R, where R is the sphere radius, a similar scaling law is obtained in the SM on the condition that the thicknesses of the external slabs (slabs 1 and 3) and of the inner slab (slab 2), namely h and d, are simultaneously multiplied by a common factor [see eqs. (30) and (31)].

<u>Remark 2</u>: The symmetric (S) or antisymmetric (A) characters of the eigenmodes of the full three-slabs system is defined with respect to the median plane of the system, namely $u(-z)=-u(z)$ and $u(-z)=u(z)$, respectively. The same symmetry property must be fulfilled by the displacement field

in the slab 2. Therefore only S-eigenmodes (resp. A-eigenmodes) of the slab 2 will contribute necessarily to the S-eigenmodes (resp. A-eigenmodes) of the three-slabs system, and will be involved in the analysis. On the other hand, S- *and* A-eigenmodes of slabs 1 and 3 will be a priori involved simultaneously in the "building-up" of the S- and A-eigenmodes of the full three-slabs system, since the character of symmetry of the displacement fields in the individual slabs is defined with respect to their respective median plane (see Figure S2). In each case, however, the same eigenmodes of slabs 1 and 3, with an equal weighting, will enter the "building-up" of the displacement field of the composite three-slabs system.

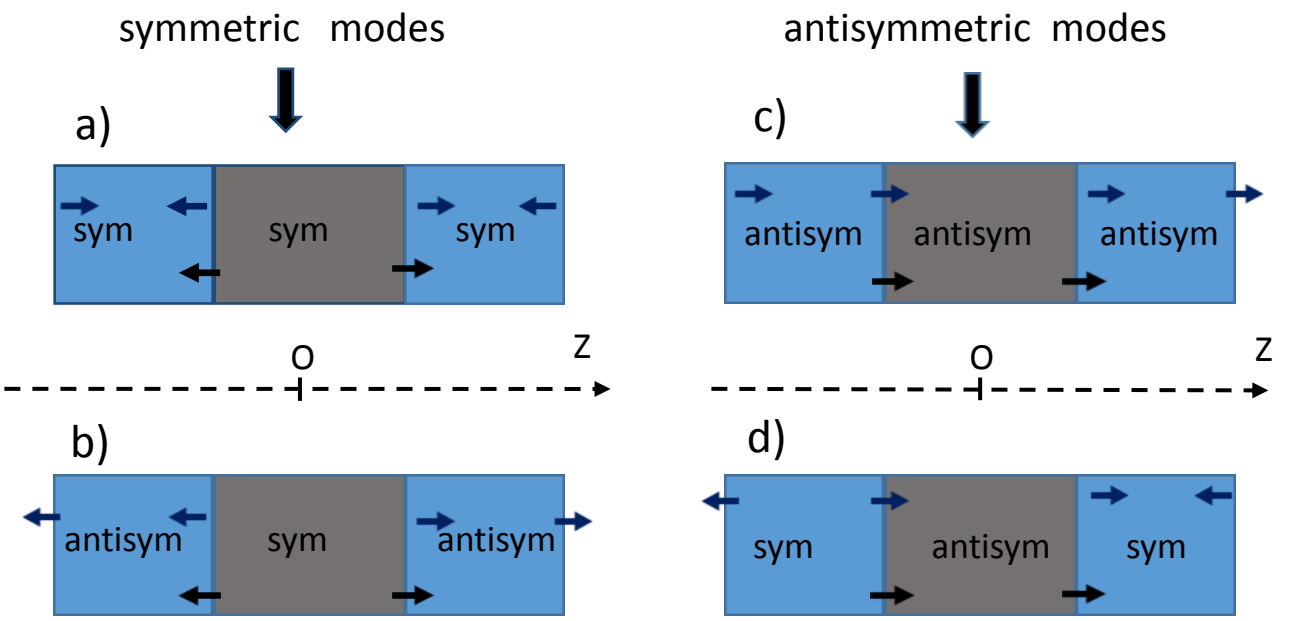

Figure S2: Figure displaying an arbitrary displacement field (symbolized by arrows in the vicinity of the four interfaces), in the case of symmetric eigenmodes [$u(-z) = -u(z)$; left panels a and b] and antisymmetric eigenmodes [$u(-z) = u(z)$, right panels c and d] of the composite multi-slabs system. In slab 1 (leftmost slab), or slab 3 (rightmost slab), the length of the two arrows (having either similar direction or opposite directions) are chosen equal in order to show that *both* symmetric and antisymmetric displacement fields inside slab 1 and slab 3 (symmetry defined here with respect to the respective median plane of each slab) can contribute to the symmetric and antisymmetric displacement fields of the full three-slabs system.

C) Results

The results are displayed in Figure S3 [only the lowest branches are shown; an infinite number of branches are solutions of eqs. (30) and (31)]. For convenience the dimensionless parameters $\xi/\pi = \omega h/\pi c_L$ and d/h are chosen to plot the results. The mechanical parameters

used in the computations are $c_L = 3642.14$ m/s , $\rho = 19.3$ kg/dm^3 (parameters appropriate to bulk gold); $c_L' = 2578.61$ m/s , $\rho' = 1.2$ kg/dm^3 [parameters appropriate to polyvinylpyrrolidone (PVP)].

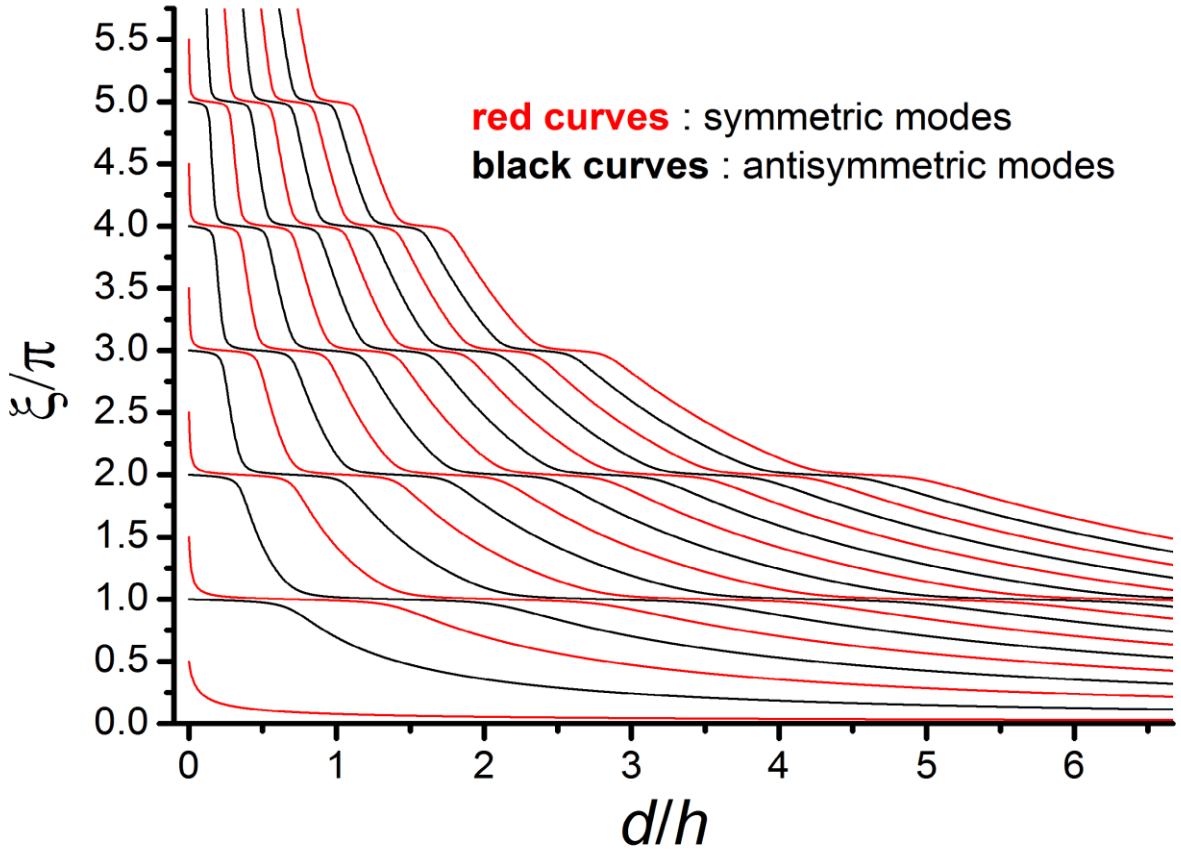

Figure S3: Red curves: symmetric modes, solutions of eq. (30). Black curves: antisymmetric modes, solutions of eq. (31). Only the lowest branches are shown.

When the ratio *d*/*h* is increased (or equivalently the slab 2 thickness *d* for a given *h* value) the eigenfrequency sets computed by solving eqs. (30) and (31) consist of continuous branches (red curves: symmetric modes; black curves: antisymmetric modes), all having a similar step-like evolution, more or less smoothed depending on the "local" ξ and/or *d*/*h* values, and evolving towards the asymptotic value $\xi = 0$ ($d/h \to \infty$). This last feature has been checked in solving eqs. (30-31) for a much more extended *d*/*h* range. This point will be discussed in Section D, when a comparison with the optical response of homodimers of spheres, as well as with the mechanical response of matrix-embedded homodimers of spheres, will be briefly addressed. The branches will be referred to, in the following, as the symmetric and antisymmetric branches.

First, we can notice that there is no crossing between the symmetric branches, as well as between the antisymmetric branches. No eigenfrequency/mode degeneracy occurs in each subset. Indeed, this is a specificity of the present one-dimensional model, where no additional "quantum number", associated with another symmetry property, can be introduced. Actually, when additional symmetry-related quantum numbers can be defined, the full problem in hand (for instance the determination of the optical or mechanical eigenfrequencies of a given nanostructure) is diagonal with respect to the different values of the quantum number labelling the symmetry, that is, the full problem split into independent "sub-problems". In such cases eigenfrequency degeneracy [in other terms branch crossings when the evolution of the eigenfrequencies as a function of a given model parameter is investigated, such as the inter-particle spacing in dimers] may occur between modes belonging to different sub-spaces. This can be inferred from Figure 1 in the Supporting Information of ref. [3] or Figure 2 in ref. [4] where bright/dark optical branches pertaining to different subsets (namely $m = 0$ and $m = 1$, where m is the azimuthal quantum number related to the axial symmetry of the homodimer of spheres) patently cross each other.

Second, there is no crossing between the symmetric and antisymmetric acoustic branches, whereas in the plasmon hybridization model in optics the branches associated with bright and dark modes (counterparts of the antisymmetric and symmetric modes of the slab model, respectively) can cross, in each individual m-subspace [3, 4]. This second feature highlights again the specificity of the present mechanical SM.

Some other descriptive remarks, concerning the step-like branch evolution, deserve to be pointed out: **(i)** along each descending branch the height of the steps between two successive flat portions are systematically on the order of unity [namely the spacing between the consecutive eigenfrequencies (in ξ/π units) of the gold slabs], whatever the descending slope is; **(ii)** along each descending branch the width of the successive flat -quasi horizontal- steps increases steadily when the branch tends towards its asymptotic zero-value (namely when d/h is enlarged); **(iii)** for a fixed ξ/π value, the spacing along the d/h coordinate between the successive descending branches is constant; **(iv)** patterns of avoided crossings between couples of branches are clearly observed.

Actually all these features can be rationalized thanks to, on the one hand the "mathematical" examination of eqs. (30) and (31), and, on the other hand, a physical analysis in terms of hybridization of the eigenmodes of the composite dimer sub-units, keeping in mind the necessary matching of the boundary conditions, displacement field and stress, at the internal interfaces (interfaces 2 and 3, located at $z = \pm d/2$).

In order to support the analysis all the eigenfrequency branches $[\xi/\pi](d/h)$, related to each sub-unit of the composite homodimer (see the caption of Figure S4 for details), have been plotted in Figure S4, together with the symmetric and antisymmetric branches of the three-slabs dimer. Figure S5 displays a magnification of a part of Figure S4.

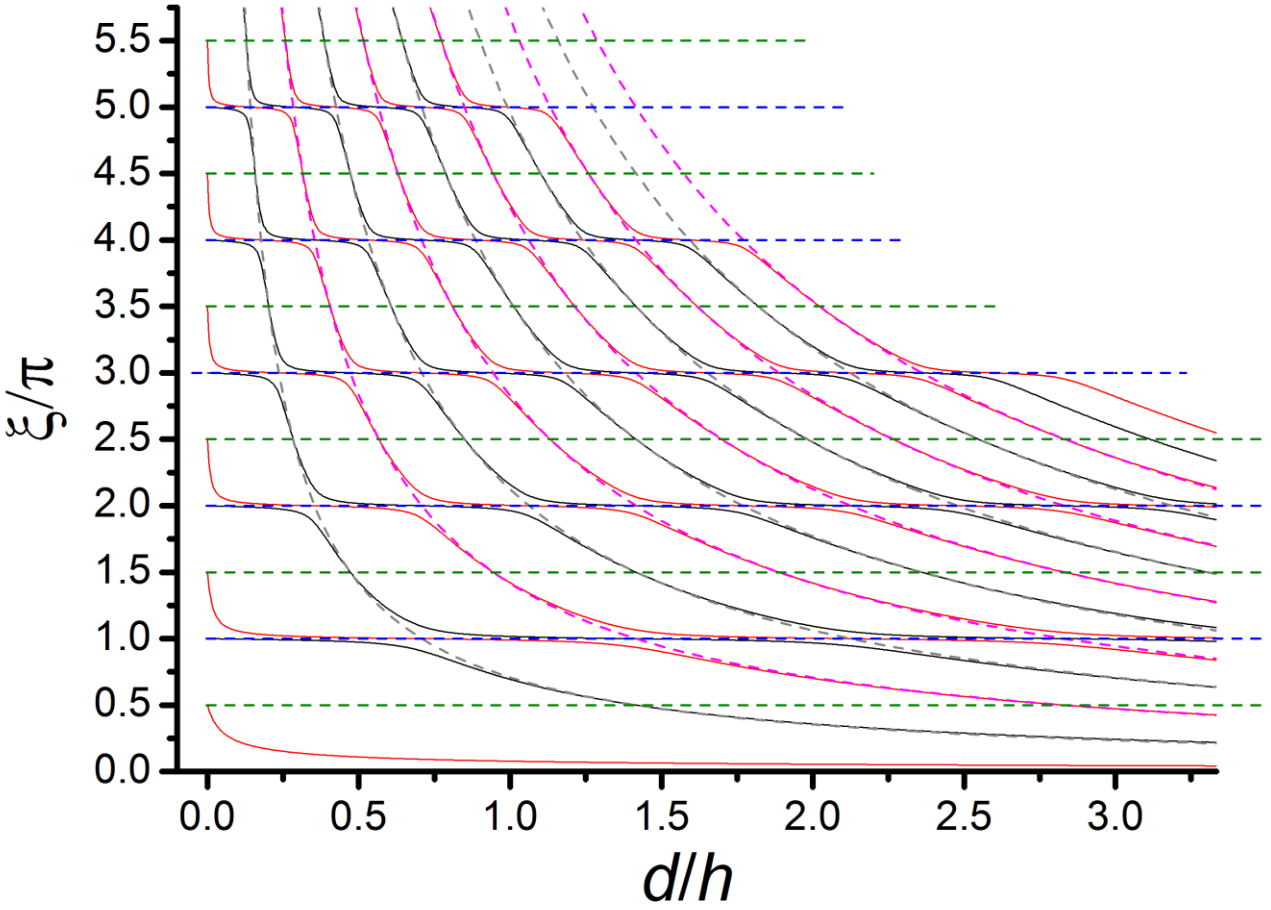

Figure S4: Full red curves: symmetric branches of the three-slabs system (homodimer), solutions of eq. (30). Black curves: antisymmetric branches of the three-slabs system (homodimer), solutions of eq. (31). Horizontal dashed blue lines: eigenfrequencies of the individual gold slabs (slabs 1 and 3 in Figure S1) characterizing eigenmodes with stress-free conditions at both interfaces [interfaces n°1 and n°2 for slab 1 ($z_1 = -h - d/2$ and $z_2 = -d/2$); interfaces n°3 and n°4 for slab 3 ($z_3 = d/2$ and $z_4 = h + d/2$)]: $\xi/\pi = n$ with n = 1, 2, 3, ….(see Section A). Horizontal dashed green lines: eigenfrequencies of the individual gold slabs (slabs 1 and 3 in Figure S1) characterizing eigenmodes with hybrid boundary conditions, namely stress-free condition at the outermost interface (z_1 for slab 1; z_4 for slab 3) and displacement-free condition at the inner PVP/gold interface (z_2 for slab 1; z_3 for slab 3): $\xi/\pi = n + 1/2$ with n = 0, 1, 2, 3, …. (see Section A). Descending dashed magenta curves: antisymmetric branches of slab 2 characterizing eigenmodes with stress-free conditions at both interfaces (z_2 and z_3) and symmetric branches of slab 2 characterizing eigenmodes with displacement-free conditions at both interfaces (z_2 and z_3): $\omega d / c_L' \pi = (\xi/\pi)(d/h)(c_L/c_L') = 2n$ with n = 1, 2, 3, …..(see Section A). Descending dashed grey curves: symmetric branches of slab 2 characterizing eigenmodes with stress-free conditions at both interfaces (z_2 and z_3) and antisymmetric branches of slab 2 characterizing eigenmodes with displacement-free conditions at both interfaces (z_2 and z_3): $\omega d / c_L' \pi = (\xi/\pi)(d/h)(c_L/c_L') = 2n + 1$ with n = 0, 1, 2, 3, …..(see Section A).

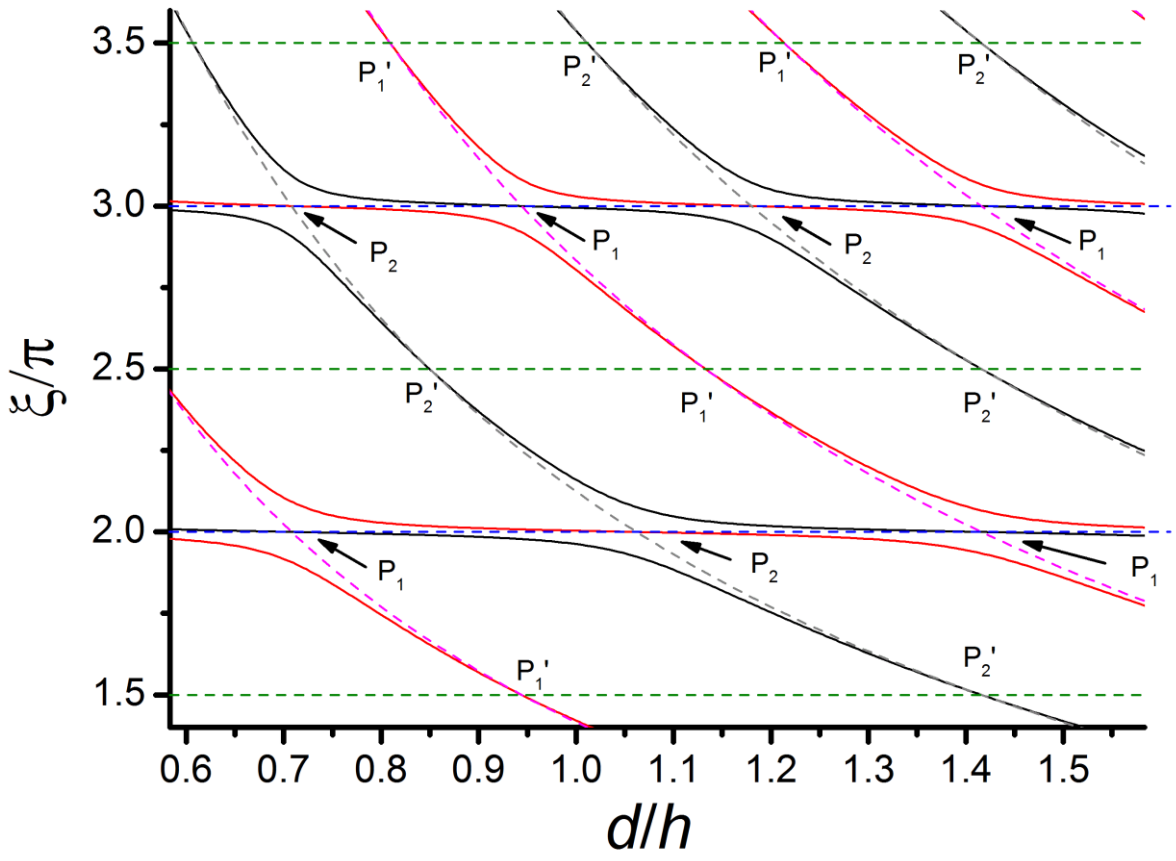

Figure S5: Magnification of a part of Figure S4.

The physical analysis of the results displayed in Figures S3-S5 can be straightforwardly conducted in noting that, for the gold/PVP system, the acoustic impedance ratio p is small (0.044), owing to the large difference between the mass densities of both materials. The step-like behavior of the branches is indeed a direct consequence of this small value. Assuming that p is very small (infinitesimal) the equations (30) and (31), the solutions of which are the frequencies of the S- and A-eigenmodes of the three-slabs system, express as

$$\sin\left(\frac{c_L}{c_L'}\frac{d}{2h}\xi\right)\sin(\xi)\approx 0 \qquad (32)$$

$$\cos\left(\frac{c_L}{c_L'}\frac{d}{2h}\xi\right)\sin(\xi)\approx 0 \qquad (33)$$

Symmetric modes (eq. 32).

For the S-eigenmodes the solutions are $\xi = n\pi$ and $(c_L / c_L')(d/h)\xi = (2n)\pi$ (with n = 1, 2, 3,….). The solutions consist therefore of the eigenmodes of the individual gold slabs (slabs 1 and 3) with stress-free conditions at both interfaces [horizontal dashed blue lines in Figures S4-S5] and of the symmetric eigenmodes of slab 2 with displacement-free conditions at both interfaces [descending magenta curves in Figures S4-S5].

The involvement of these specific solutions for very small impedance ratios has a simple physical explanation, that can be inferred without resorting to any mathematical analysis, in recalling that vibrational eigenmodes are self-sustained periodic motions (obviously, if no strong dissipative mechanism is present) that can be launched for instance, either by a tiny fluctuation of the mechanical coupling with the "environment", or by an impulse $\delta(t)$-type excitation of the electron gas in the case of metallic nanostructures, as done in time-resolved pump-probe spectroscopy experiments [5]. If the localized excitation affects primarily the gold slabs, it is expected that their eigenmodes with stress-free conditions ($\xi = n\pi$) will be launched since the intermediate slab 2 ($\rho' \approx 0$) behaves as the vacuum for the heavy gold slabs 1 and 3. In this case the displacement field of slab 2 is enslaved to those of the outermost slabs 1 and 3. On the other hand, if the localized excitation affects primarily the intermediate slab 2, it is expected that its symmetric eigenmodes with displacement-free conditions at both interfaces $z = \pm d/2$ [$(c_L / c_L')(d/h)\xi = (2n)\pi$] will be launched since the outermost slabs 1 and 3 ($\rho >> \rho'$) behave as rigid walls for the light intermediate slab 2. In this case the displacement fields of slabs 1 and 3 are enslaved to that of the inner slab 2.

It should be pointed out that, even in the case of very small *p*-values (in particular when $\rho'/\rho <<< 1$), the crossing points between the horizontal dashed blue lines and the descending magenta curves (points labelled P_1 in Figure S5) do not belong to the symmetric branches of the three-slabs system since stress-free and displacement-free boundary conditions cannot be simultaneously fulfilled at the interfaces $z = \pm d/2$. This incompatibility is at the origin of the "avoided-crossing patterns" observed in Figures (S3-S5).

Antisymmetric modes (eq. 33).

For the A-eigenmodes the solutions are $\xi = n\pi$ (with n = 1, 2, 3, …) and $(c_L / c_L')(d/h)\xi = (2n+1)\pi$ (with n = 0, 1, 2, 3,….). The solutions consist therefore of the eigenmodes of the individual gold slabs (slabs 1 and 3) with stress-free conditions at both interfaces [horizontal dashed blue lines in Figures S4-S5] and of the eigenmodes of slab 2 with displacement-free conditions at both interfaces [descending grey curves in Figures S4-S5]. Similar physical discussion and analysis can be conducted for supporting the two sets of antisymmetric solutions. As previously the crossing points between the horizontal dashed blue lines and the descending grey curves (points labelled P_2 in Figure S5) do not belong to the antisymmetric branches of the three-slabs system since stress-free and zero-displacement boundary conditions cannot be simultaneously fulfilled at the interfaces $z = \pm d/2$.

When *p* is slightly enlarged (*p*-value of the gold/PVP system for instance) the branches of the full three-slabs system move away noticeably from the eigenfrequency branches associated with the sub-units of the full composite system (see Figures S4 and S5). Nevertheless they remain clearly organized along the branches involved previously for studying the asymptotic case $p \to 0$ (and in their close vicinity). All the branches become clearly distinguishable, all having a step-like behaviour, with no crossing between the different branches. Moreover the whole branch pattern in the $(\xi/\pi, d/h)$ plane exhibits conspicuous avoided-crossing patterns between couples of S-branches (at the points P_1) and between couples of A-branches (at the points P_2).

Additional physical information can be obtained from Figures S4 and S5 in noting that three branches intersect at the points P_1 [(i) a horizontal dashed blue line, (ii) a descending magenta

curve, (iii) an antisymmetric branch of the full three-slabs system], and three branches intersect at the points P_2 [(i) a horizontal dashed blue line, (ii) a descending grey curve, (iii) a symmetric branch of the full three-slabs system]. Indeed at the points P_1 the corresponding antisymmetric eigenmode of the three-slabs system is built up from the mere juxtaposition of eigenmodes of the three individual slabs (same frequency and stress-free boundary conditions). Remark that the eigenmode of the intermediate slab 2 is (necessarily) antisymmetric, whereas those of the outermost gold slabs 1 and 2 can be symmetric or antisymmetric (see Figure S2). So points P_1 lie on every horizontal dashed blue line $\xi/\pi = n$ (n = 1, 2, 3, …). Similarly at each point P_2 the corresponding symmetric eigenmode of the three-slabs system is built up from the mere juxtaposition of eigenmodes of the three individual slabs (same frequency and stress-free boundary conditions).

Two other remarkable sets of points (P_1' and P_2' in Figure S5), involving the crossing of three branches, provide also physical insights about the nature of the displacement field characterizing the corresponding eigenmodes. At the points P_1' the three following branches intersect: (i) a horizontal dashed green line ($\xi/\pi = n+1/2$ with n = 0, 1, 2, 3,….), (ii) a descending magenta curve, (iii) a symmetric branch of the full three-slabs system. At these points the corresponding symmetric eigenmode of the three-slabs system is built up from the mere juxtaposition of a symmetric eigenmode of slab 2 of same frequency with displacement-free boundary condition at both interfaces $z = \pm d/2$ and identical eigenmodes of slabs 1 and 3 (same frequency and hybrid boundary conditions: stress-free at the outermost interfaces $z = \pm(d/2 + h)$, displacement-free at the inner interfaces $z = \pm d/2$). A similar analysis can be conducted for the antisymmetric modes of the three-slabs system corresponding to the points P_2'.

D) Hybridization analysis :

Before presenting illustrative results for the SM it is worthwhile recalling briefly the general lines of the popular plasmon hybridization (PH) model introduced in optics to compute the optical response of homodimers consisting of identical electrostatically-coupled spheres (actually the PH model can be applied to any other metal nanostructures) [3, 4, 6]. These preliminaries are of main importance to highlight the specificity of the PH-like approach in the case of the SM.

In the PH model the conduction electron gas in each sphere is described as a homogeneous negatively charged incompressible fluid (neutralized by a homogeneous positively charged ionic background, of *jellium*-type), the shape fluctuations of which (departure from the perfect spherical symmetry) give rise to a net surface charge density which, mathematically, can be written as the sum of multipolar contributions [expansion over the scalar harmonics $Y_\lambda^m(\theta,\phi)$], namely

$$\sigma_s(\theta,\phi) = \sum_{\lambda,m} C_{\lambda,m} Y_\lambda^m(\theta,\phi) \qquad (34)$$

For an isolated single sphere, to each self-sustained electron gas excitation (eigenmodes named plasmons) is associated a specific multipolarity (λ, m) of the surface charge density [eigenfrequency $\omega_{\lambda,m}$; surface charge density $\sigma_s^{\lambda,m}(\theta,\phi) \propto Y_\lambda^m(\theta,\phi)$]. In the case of a homodimer (d is the inter-sphere distance; the z-axis is chosen along the line connecting the centres of both spheres) the electrostatic coupling between the two surface charge densities on the surfaces of both spheres leads to eigenmodes of the two-spheres system, either symmetric (S) or antisymmetric (A), characterized by surface charge densities involving all the multipolarities (λ, m). In fact, because of the axial symmetry of the homodimer, the full problem is diagonal with respect to m ("good" quantum number). So, each eigenfrequency can be labelled in addition to the S/A symmetry by the index m

[namely $\omega_{m,k}^{S/A}(d)$]. For each eigenmode and distance *d*, the surface charge densities in each sphere *i* (*i* = 1 or 2) can be expanded in the form

$$\sigma_{m,k}^{d,S/A}(\theta_i,\phi_i)=\sum_{\lambda} C_{\lambda,m}^{k,S/A}(d)\sigma_s^{\lambda,m}(\theta_i,\phi_i) \qquad (35)$$

The above expansions upon the surface charge densities characterizing the eigenmodes of the monomers (isolated spheres), which express the mixing of the electron gas eigen-excitations of the monomers induced by the inter-spheres electrostatic coupling, is what is termed "plasmon hybridization". We can note that the surface charge densities associated with the eigen-excitations of the monomers constitute a complete basis for the general expansion eq. (35). Moreover, in the context of optics, each eigenfrequency branch $\omega_{m,k}^{S/A}(d)$ converges towards a specific eigenfrequency $\omega_{\lambda,m}$ of the monomer owing to the "fast" decrease of the inter-spheres electrostatic coupling when the distance *d* is enlarged.

In the present case [three-slabs system (or any other *finite* composite nanostructures) in vacuum] the physical problem is indeed not similar. Even though two identical gold slabs are involved (or two cylinders, or two spheres; see the main text) the terminology "homodimer" must to be viewed with great caution. Indeed this terminology is to a large extent misleading if a strict reference to the PH approach developed for determining the plasmonic excitations of metal dimers is made. Strictly the terminology "three-slabs system" would be more appropriate. The reason is that the physics of such finite mechanical systems (the SM has also a finite extent with respect to the motion along the *z*-axis) cannot be paralleled with that of homodimers in the context of optics. Independently of their respective context (optics and mechanics) the physics differ in many respects. First the acoustic eigenfrequency branches of the "homodimer" do not converge towards the eigenfrequencies of the individual gold slabs because the slab 2-mediated mechanical coupling remains efficient even at very large spacings *d*. There is no dissipation of the energy stored in the acoustic longitudinal waves launched by both external slabs in the intermediate slab 2. In other words the motion of each gold slab affects the motion of the other at any spacing *d*. Moreover, even in the presence of viscosity in slab 2, the branches would converge to finite values unrelated to the eigenfrequencies of the individual gold spheres in vacuum. As a matter of fact, for each value of the slab 2 thickness, one is faced with a novel mechanical system, and not with a homodimer in the usual physical sense defined in the context of optics.

The second encountered "problem" is more technical and concerns the physical quantity associated with the "three-slabs system" to be selected for conducting a PH-like analysis, allowing expansions of the form eq. (35) to be established. Clearly the only physical quantity available for fulfilling this purpose is the displacement field in a single gold slab (slab 1 for instance). The "problem" is rooted in the fact that different boundary conditions are involved for dealing with, in the one hand a single gold slab in vacuum, and, on the other hand a gold slab belonging to the "three-slabs system" (the boundary conditions differ at the internal interface $z=-d/2$). The consequence is that a general displacement field in slab 1 cannot be expanded on the whole (infinite) set of displacement fields associated with the eigenmodes of the isolated slab [stress-free boundary conditions at both interfaces; $[\partial u_1/\partial z](z=\pm h/2)=0$]. Indeed none of the three sets introduced in Section A for different couples of boundary conditions [Case 1); Case 2) and Case 3)] are complete from a mathematical point of view (that is, none of them constitutes a complete basis for expanding any arbitrary one-dimensional displacement field). Moreover the displacement fields belonging to a given set are not orthogonal to each displacement field belonging to another set. For instance the integral of the products of symmetric (or antisymmetric) modes of Cases 1) and 2) over the slab thickness [$z = -h/2$, $z = h/2$] are different from zero.

Nevertheless, expansions upon a particular *pseudo-basis* provide physical information of major interest about the evolution of the eigenmode displacement field of slab 1 (and in consequence of slab 3, because of the global symmetry of the modes) over an extended spacing range (inter-slab separation *d*). For instance, in the vicinity of the points P_1 and P_2 in Figure S5, we can infer that only one (or a few) monomer eigenmodes of Case 1) (stress-free boundary conditions) contribute to the displacement field in slab 1, but many of them are probably involved in the descending portions of the branches (grey or magenta curves, depending on the symmetry of the branches). On the other hand one (or a few) monomer eigenmodes of Case 3) (hybrid boundary conditions) are expected to contribute in the vicinity of the points P_1' and P_2' (see Figure S5)

By way of illustration we present PH-like expansions of the displacement field in slab 1 for the eigenmodes belonging to two branches plotted in Figures S3 [one symmetric (S) and one antisymmetric (A)], in using the *pseudo-basis* of Case 1) (stress-free boundary conditions; eigenmodes of a single gold slab in vacuum). For this purpose we need first to express the normalized displacement field in slab 1 for each eigenfrequency $\xi^{S/A}(d/h)$. From eq. (17) the displacement field in slab 1 expresses as

$$u_1(z) = A_1[\cos(\xi^{S/A}(d/h)\frac{z}{h}) + \frac{B_1}{A_1}\sin(\xi^{S/A}(d/h)\frac{z}{h})] \tag{36}$$

For both S- and A-eigenmodes one has (see Section B)

$$\alpha^{S/A}(d/h) = \frac{B_1}{A_1} = -tg(\xi^{S/A}(d/h)\frac{a}{2h}) \quad \text{(with } a = d + 2h\text{)} \tag{37}$$

The normalized displacement field in slab 1 is thus

$$\bar{u}_{\xi^{S/A}(d/h)}(z) = \frac{f(z)}{\sqrt{\int_{-a/2}^{-d/2} |f(z)|^2 dz}} \tag{38}$$

with

$$f(z) = \cos(\xi^{S/A}(d/h)\frac{z}{h}) + \alpha^{S/A}(d/h)\sin(\xi^{S/A}(d/h)\frac{z}{h}) \tag{39}$$

It is worthwhile recalling that in the previous equations, eqs. (36), (38) and (39), the coordinate *z* is measured relative to the transverse median *x-y* plane of the three-slabs system (see Figure S1).

The normalized displacement fields of the symmetric and antisymmetric eigenmodes of a single slab in vacuum [Case 1); stress-free boundary conditions] are given by eqs. (7) and (8), namely

S-modes $\bar{u}_n(z) = \sqrt{\frac{2}{h}}\sin(\frac{n\pi}{h}z)$ (*n* odd) (40)

A-modes $\bar{u}_n(z) = \sqrt{\frac{2}{h}}\cos(\frac{n\pi}{h}z)$ (*n* even) (41)

where in eqs. (40 and (41) the coordinate *z* is measured with respect to the transverse median *x*-*y* plane of the slab (see Figure S1).

Finally the PH-like expansions of $\bar{u}_{\xi^{S/A}(d/h)}(z)$ [the counterpart of eq. (35)] is conveniently characterized by computing the following square integrals (which will be termed "populations" in the following)

$$p_n^{S/A}(d/h) = \left| \int_{-h/2}^{h/2} \bar{u}_{\xi^{S/A}(d/h)}(z - h/2 - d/2)\, \bar{u}_n(z) dz \right|^2 \tag{42}$$

The results are displayed in Figure S6 for two selected branches. Magnifications for small *d*/*h* values, in selected ranges where several populations of low weight contribute to the expansion, are provided in Figure S7. Both figures give strong support to the previous comments and analyses of the full branch patterns in Figures S4 and S5. In addition we have checked analytically that at the crossing points P_1 and P_2 (see Figure S5) the populations $p_n^{S/A}(d/h)$ are strictly zero, except that of the *n*-value characterizing the horizontal dashed blue line crossing the points (for this specific value $p_n^{S/A}(d/h) = 1$).

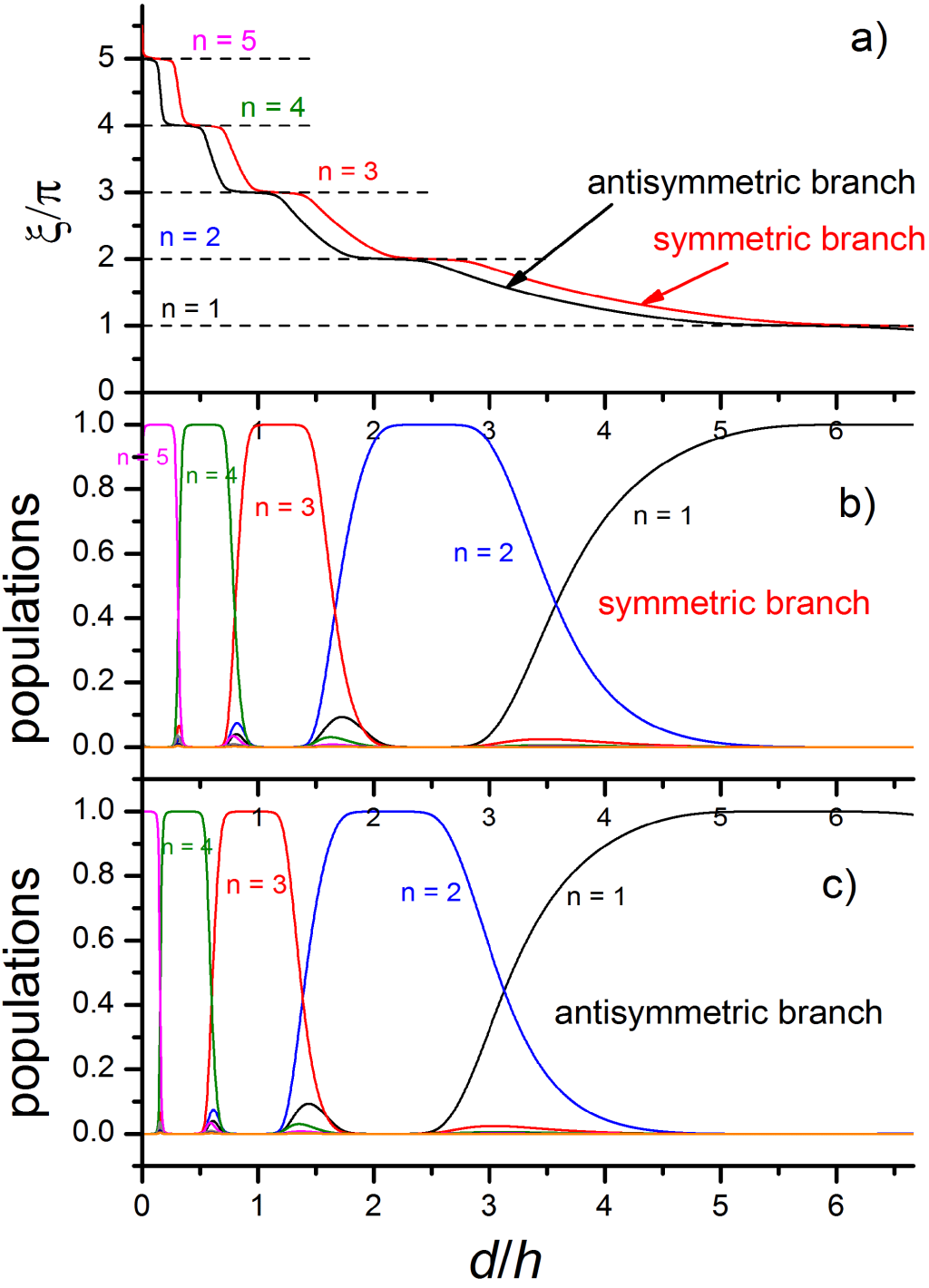

Figure S6: Hybridization analysis of two eigenfrequency branches displayed in Figure S3 and S4. a) Red curve: symmetric branch. Black curve: antisymmetric branch. b) Populations $p_n^S(d/h)$ [eq. (42)] of the symmetric branch. c) Populations $p_n^A(d/h)$ of the antisymmetric branch [eq. (42)].

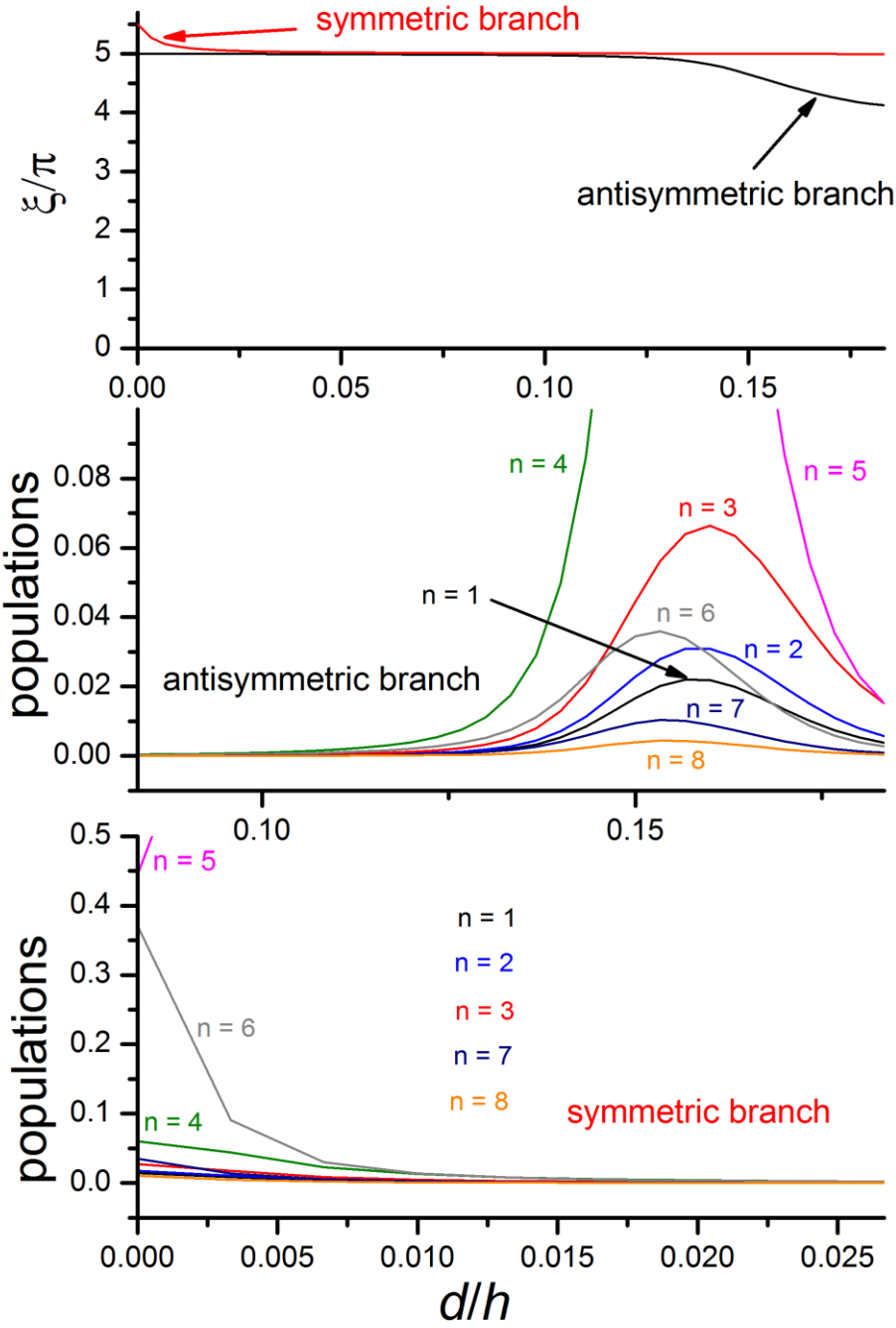

Figure S7: Magnification of parts of Figure S6, for small values *d*/*h*. Note that different vertical scales and *d*/*h*-ranges are involved in the two lower panels.

To conclude this Section it should be emphasized that a PH-like description, quite similar to the PH model developed in optics for metal particle homodimers, free from the preceding drawbacks, can be built up for a system of two identical spheres embedded in an *infinite* elastic matrix (work in course of preparation). In this system the energy of the spherical elastic waves launched by the vibrating spheres are efficiently "dissipated" in the surrounding infinite matrix (*geometrical* mechanism), more precisely are evacuated from the inter-spheres region ruling the

mechanical coupling, when d is enlarged. Two factors are responsible of the fast decrease of the inter-spheres mechanical coupling: (i) at large distances the displacement field of the emitted spherical waves scales as $1/D$ where D is the distance from the sources emitting the waves; (ii) the solid angle subtending the surface of the spherical wave emitted by a given sphere, that efficiently impact mechanically the other sphere, scales as $1/D^2$. So, the effective mechanical coupling between both spheres vanishes at large enough inter-particles distances and the eigenfrequency branches of the two-spheres system converge towards the Lamb modes of the isolated spheres. In addition, since the boundary conditions at the sphere/matrix interfaces are the same for isolated matrix-embedded spheres and the spheres belonging to the dimer, the displacement fields of the eigenmodes of the monomers constitute a complete basis for expanding the displacement field in both spheres of the dimer.

E) Dependence of coupled vibrational modes on the impedance acoustic ratio *p*.

Actually the conspicuous step-like behavior of the eigenfrequency branches displayed in Figures S3-S5 is the consequence of the small value of the acoustic impedance ratio p for the gold/PVP system, as already stated. Strong changes of the overall branch pattern occur when this ratio is enlarged. By way of illustration Figure S8 shows the full branch pattern computed in just increasing the mass density ρ' of the material in slab 2 (the longitudinal sound velocity of PVP is retained in these calculations). When ρ' is enlarged the eigenfrequency branches flatten noticeable, especially in the vicinity of the avoided crossing patterns (located around the points P_1 and P_2 in Figure S5), and, for much larger mass densities, the initial step-like behaviors of the branches are only reflected through smooth oscillations.

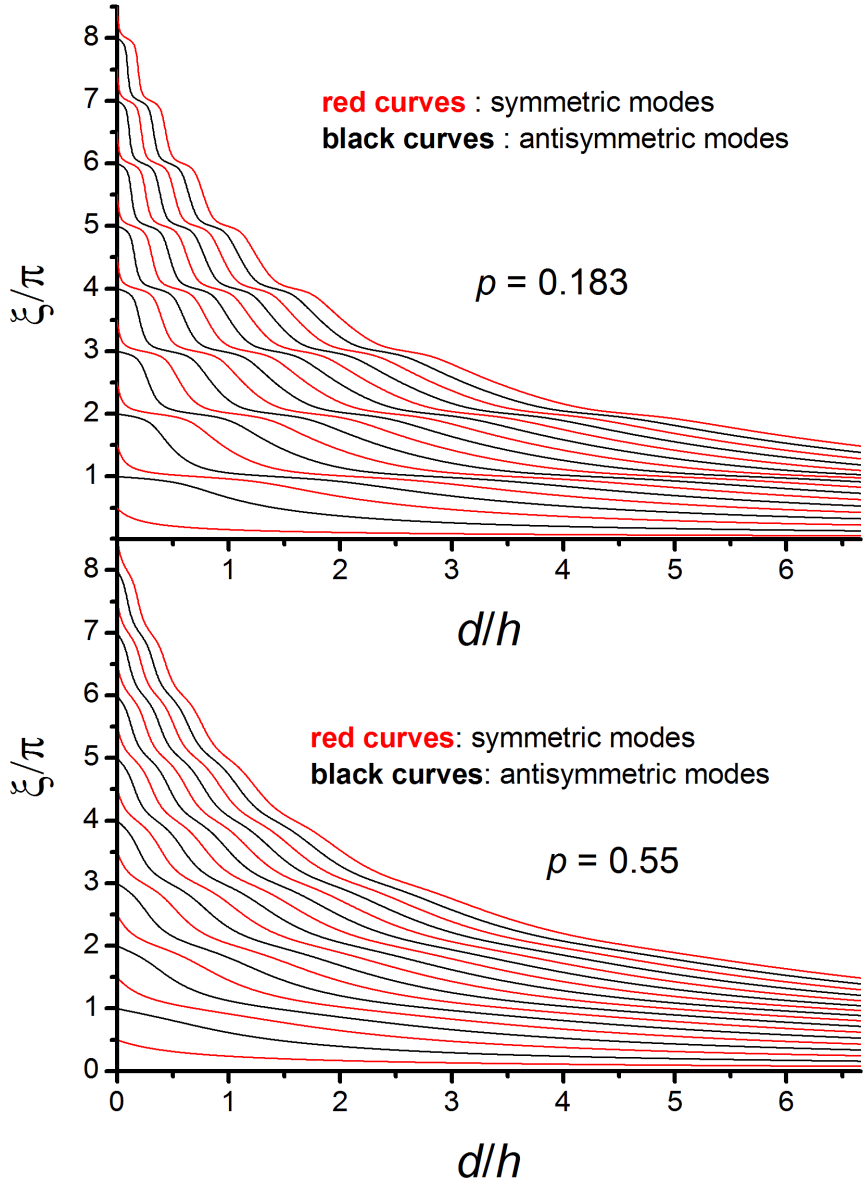

Figure S8: Evolution of the full eigenfrequency branch pattern as a function of the acoustic impedance ratio *p*. This ratio has been changed in our numerical code in just modifying the mass density of the material in slab 2. The longitudinal sound velocity of PVP, c_L' = 2578.61 m/s, is used in the calculations. Upper panel: ρ' = 5 kg/dm^3 ($\rightarrow p$ = 0.1834). Lower panel: ρ' = 15 kg/dm^3 ($\rightarrow p$ = 0.5502).

Some final remarks deserve to be added concerning the number of independent parameters entering the SM, essentially because the results have been displayed *for convenience* in using dimensionless parameters, namely ξ, d/h and p. Let us stress that both the mass density ratio (through the acoustic impedance ratio p) *and* the longitudinal sound velocity ratio c_L / c_L' (see eqs. 30-31) are relevant parameters. So, for a given material in slabs 1 and 3, *both* the mass density and longitudinal sound velocity in the intermediate slab 2 matter. Since the longitudinal sound velocity c_L enters the definition of the dimensionless eigenfrequency parameter $\xi = \omega h / c_L$ *three* material parameters among four (mass densities and longitudinal sound velocities) determine the eigenfrequencies (in Hz) for a given geometry (d and h). Finally, since h, the thickness of the

external slabs 1 and 3, enters also the definition of ξ, the eigenfrequencies (in Hz) of the three-slabs system are ruled by five effective independent parameters.

The strong dependence of the symmetric eigenmodes on the spacing between two very close nanostructures (*d*/*h* close to zero in the present slab model) could be used to develop highly sensitive mechanical sensors at the nanoscale [see for instance the experimental work in Ref. [5] (time-resolved pump-probe spectroscopy experiment) which involves chemically synthesized hexagonal and triangular nanoplates]. To illustrate this dependence Figure S9 shows the *d*/*h*-evolution of the eigenfrequencies belonging to two close branches (one symmetric and one antisymmetric) located in the bottom part of Figure S3. We have selected these low-frequency branches because they are expected to be more easily probed experimentally in comparison with those of higher frequencies. The various curves have been computed in just modifying the mass density ρ' of the material in slab 2 (the longitudinal sound velocity of PVP, c_L' = 2578.61 m/s, is used in the calculations), in the range 1.2 kg/dm^3 ↔ 20 kg/dm^3 (*p* varies in the range 0.044 ↔ 0.734).

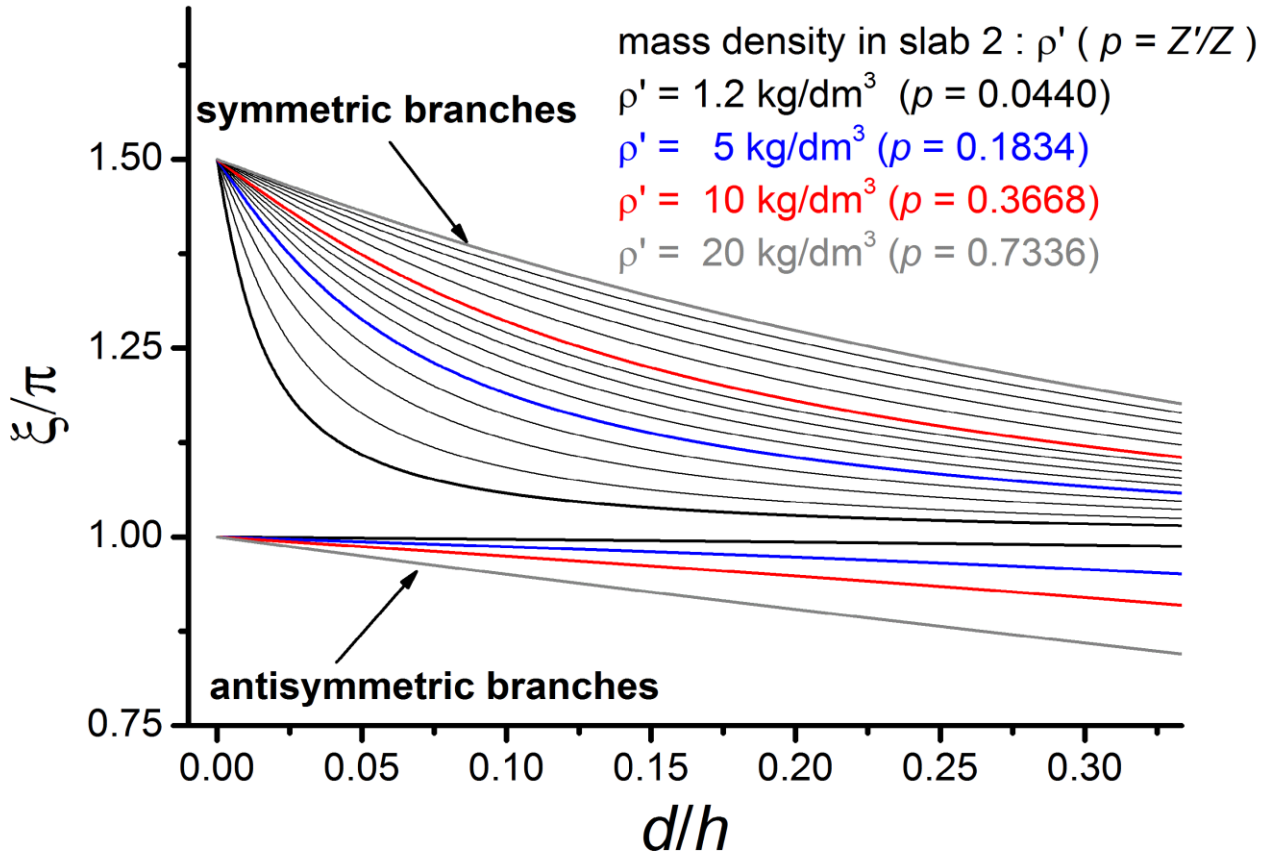

Figure S9: Dependence of the lowest symmetric and antisymmetric branches on the acoustic impedance ratio *p*. *p* has been increased as compared to the reference Au-PVP case by just modifying the mass density ρ' of the material in slab 2, in the range 1.2 kg/dm^3 ↔ 20 kg/dm^3 (*p* varies in the range 0.044 ↔ 0.734). ρ' = 1.2, 2, 3, 4, 5, 6, 7, 8, 9 10, 12, 14, 16, 18, 20 kg/dm^3. For clarity only four antisymmetric branches have been plotted.

Expanding eqs. 30 and 31 about $d/h \approx 0$, and keeping only the lowest order in the expansion (the first-order approximation holds if $\xi(d) - \xi(0) << \pi$), allows to estimate the eigenfrequencies in the spacing range of interest ($d/h \approx 0$) as a function of the SM parameters

Symmetric modes:

$$\frac{\xi}{\pi} = \frac{\omega h}{\pi c_L} = (n + \frac{1}{2})\,(1 - \frac{c_L}{2c_L'}\frac{d}{h}\frac{1}{p}) = (n + \frac{1}{2})\,(1 - \frac{1}{2}\frac{\rho}{\rho'}(\frac{c_L}{c_L'})^2\frac{d}{h}) \qquad (43)$$

Antisymmetric modes:

$$\frac{\xi}{\pi} = \frac{\omega h}{\pi c_L} = n\,(1 - \frac{c_L}{2c_L'}\frac{d}{h}p) = n\,(1 - \frac{1}{2}\frac{\rho'}{\rho}\frac{d}{h}) \qquad (44)$$

The branches shown in Figure S9 correspond to the value $n = 1$.

References

[1] Eringen, A. C.; Suhubi, E. S. *Elastodynamics Vol. II: Linear Theory*; Academic Press, New York, 1975.

[2] Crut, A.; Maioli, P.; Del Fatti, N.; Vallée, F. Acoustic Vibrations of metal nano-objects: Time-domain investigations. *Phys. Rep*. **2015**, *549*, 1-43.

[3] Lermé, J. Nanoparticle above a Dielectric Interface: Plasmon Hybridization Model, Comparison with the Dimer System and against Exact Electrodynamics Calculations. *J. Phys. Chem. C* **2014**, *118*, 28118-28133.

[4] Lermé, J. Plasmon Hybridization Model for a Nanoparticle above a Dielectric Interface: Dielectric Effects, Comparison with the Dimer System, Range of Applicability and Limits. *J. Phys. Chem. C* **2015**, *119*, 21087-21104.

[5] Wang, J.; Yu, K.; Yang, Y.; Hartland, G.V.; Sader, J. E.; Wang, G.P. Strong vibrational coupling in room temperature plasmonic resonators. *Nature Comm*. **2019**, *10*, 1-8.

[6] Nordlander, P.; Oubre, C.; Prodan, E.; Li, K.; Stockman, M.I. Plasmon Hybridization in Nanoparticle Dimers. *Nano Lett*. **2004**, *4*, 899-903.

Vibrations of coupled spheres (see Figure 3 in the main text)

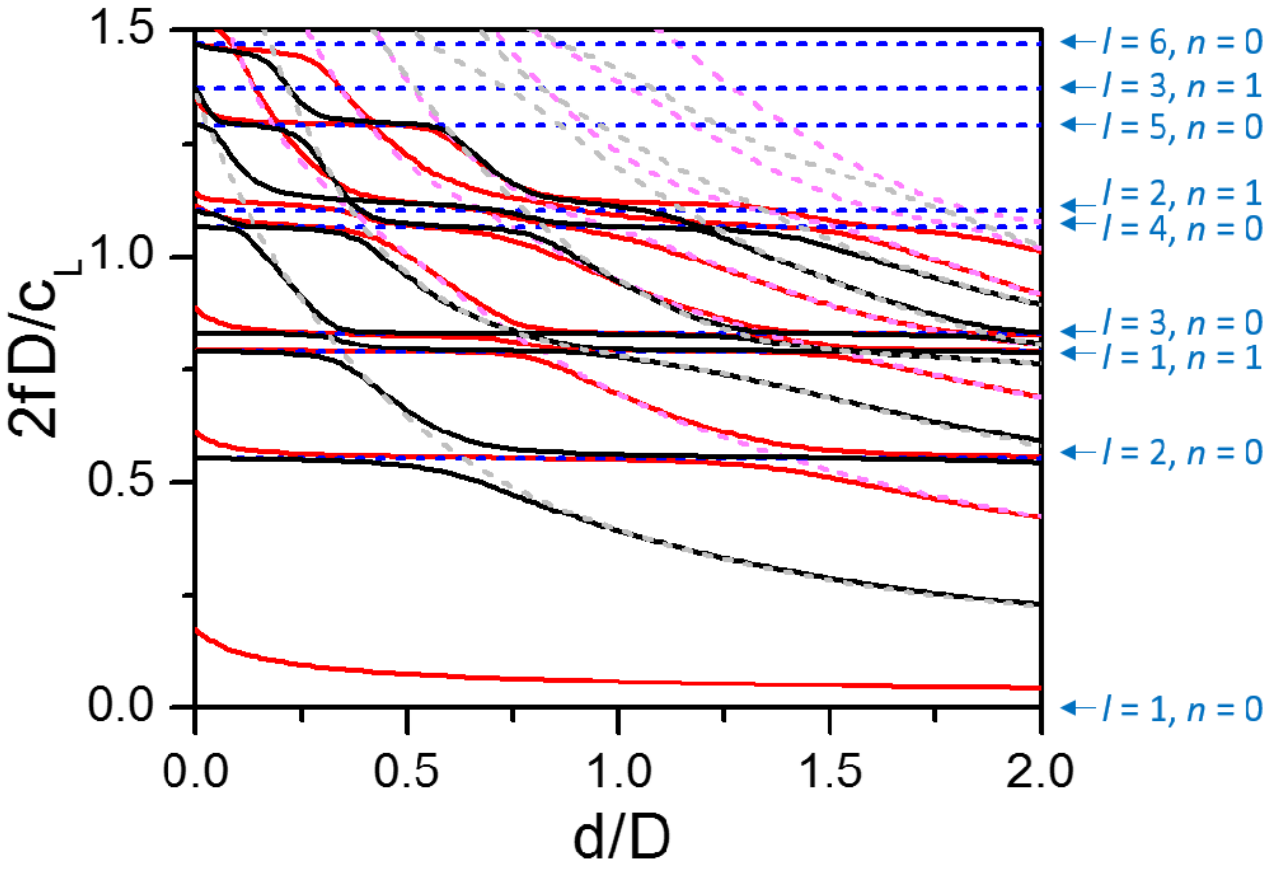

Figure S10: Vibrational eigenfrequencies computed using FEM for the symmetric (red curves) and antisymmetric (black curves) modes of gold spheres mechanically coupled by a PVP spacer. The eigenfrequencies of isolated components are shown as dashed blue horizontal lines (gold sphere Lamb modes, computed with stress-free BCs on the sphere surface) and dashed magenta/grey curves (symmetric/antisymmetric modes of the PVP spacer, computed with displacement-free BCs at the hemispherical ends, and stress-free BCs on its lateral cylindrical surface. The geometry of the coupled sphere system is depicted in the main text (Figure 3), as well as the low-frequency part of the eigenfrequency branch pattern.